

Percolative transition on ferromagnetic insulator manganites: Uncorrelated to correlated polaron clusters

A. M. L. Lopes,^{1,2,*} J. P. Araújo,³ J. J. Ramasco,⁴ V. S. Amaral,² R. Suryanarayanan,⁵ and J. G. Correia^{1,6}

¹The ISOLDE Collaboration, CERN EP, CH 1211 Geneva 23, Switzerland

²Departamento de Física and CICECO, Universidade de Aveiro, 3810-193 Aveiro, Portugal

³Departamento de Física and IFIMUP, Universidade do Porto, 4169-007 Porto, Portugal

⁴Physics Department, Emory University, Atlanta, Georgia 30322, USA

⁵Laboratoire de Physico-Chimie et de l'Etat Solide, Université Paris-Sud, 91405 Orsay, France

⁶ITN, E.N. 10, 2686-953 Sacavém, Portugal

(Received 2 February 2006; published 24 March 2006)

We report an atomic-scale study on the ferromagnetic insulator manganite $\text{LaMnO}_{3,12}$ using γ - γ perturbed angular correlation spectroscopy. Data analysis reveals a nanoscopic transition from an undistorted to a Jahn-Teller (JT) distorted local environment upon cooling. The percolation thresholds of the two local environments enclose a macroscopic structural transition (rhombohedral-orthorhombic). Two distinct regimes of JT distortions were found: a high-temperature regime where uncorrelated polaron clusters with severe distortions of the Mn^{3+}O_6 octahedra survive up to $T \approx 800$ K and a low-temperature regime where correlated regions have a weaker JT-distorted symmetry.

DOI: [10.1103/PhysRevB.73.100408](https://doi.org/10.1103/PhysRevB.73.100408)

PACS number(s): 75.47.Lx, 31.30.Gs, 64.60.Ak, 76.80.+y

Intense experimental and theoretical work has been devoted to manganite systems due to their colossal magnetoresistance (CMR), polaron dynamics, and charge-orbital ordering phenomena. The undoped manganites (AMnO_3 where A is a trivalent ion of La, Pr, ...) typically show antiferromagnetic insulator behavior and cooperative Jahn-Teller (JT) distortion of MnO_6 octahedra. Oxygen excess or the presence of divalent ions at A sites reduce the static JT distortion by the creation of Mn^{4+} ions. This effect favors the ferromagnetic interaction via dynamic electron transfer between Mn^{3+} and Mn^{4+} , the so-called double-exchange (DE) interaction.¹ Although DE interaction explains qualitatively the CMR, it does not fully account for the large resistivity of the paramagnetic and ferromagnetic insulator phases. Polaron formation must certainly play an important role in this respect.²⁻⁵ Polarons are formed due to the strong electron-lattice coupling that leads to charge localization via JT distortions. Recently, the nature of such local distortions, their dynamics and correlations have been addressed by several authors.⁶⁻¹¹ In spite of such an effort, several issues as the detailed structure of polarons, the temperature evolution of polaron clusters, or the effect of such evolution on the average macroscopic lattice structure still remain as open questions.

Local distortions and their dynamics can be studied by using γ - γ perturbed angular correlation spectroscopy (PAC), a nuclear hyperfine method specially effective to sample atomic-scale environments. PAC efficiency is T independent, allowing us to explore a wide range of temperatures. To gain further insight on the microscopic nature of polaronic distortions, their spatial correlations, and the role of polarons in ferromagnetic insulator manganites (FMI), we have studied in detail the compound $\text{LaMnO}_{3,12}$ using the PAC technique. This compound is a prototypical FMI manganite that undergoes a rhombohedral (R)-orthorhombic (O) structural transition around room temperature, which provides us with an ideal scenario to probe the evolution of local lattice distortions through different average lattice symmetries. In par-

ticular, we show that random distributed polaron clusters survive in the undistorted R phase up to temperatures as high as 776 K. These distortions are as strong as those observed in the orbital ordered LaMnO_3 . Lowering T , the clusters continuously expand until a microscopic transition takes place at $T_s \approx 170$ K. Below the transition, the distortions are accommodated into a weaker JT-distorted phase.

$\text{LaMnO}_{3+\Delta}$ [$\Delta=0.00(2)$, $0.08(1)$, and $0.12(1)$] polycrystalline samples were produced by the solid-state reaction method. Powder x-ray diffraction measurements show that the samples are chemically homogeneous. In agreement with Refs. 12 and 13, we find an antiferromagnetic insulator ground state for the orthorhombic JT-distorted $\Delta=0$ compound ($T_N \approx 139$ K), a ferromagnetic insulator behavior for the weakly distorted $\Delta=0.08$ sample ($T_c \approx 150$ K), and a ferromagnetic insulator state for the compound with $\Delta=0.12$ ($T_c \approx 145$ K). This latter system presents as well an O - R phase transition around room temperature. As shown in Refs. 12 and 14, the oxygen excess Δ results in equivalent amounts of La and Mn vacancies, with the fraction of Mn^{4+} equal to 2Δ . γ - γ PAC measurements were performed using a high-efficiency 6-BaF₂ detector spectrometer.¹⁵ PAC samples (one per measurement) were implanted at room temperature with ^{111m}Cd to a homogeneous low dose of 10^{12} cm⁻² at 60 keV in the ISOLDE/CERN facility. Remaining point defects created during implantation were eliminated by annealing at 700 °C under an O₂ controlled atmosphere for 20 min. The peak density of probing Cd only attains 1 ppm of the La concentration. Consequently, the implanted Cd atoms are simply incorporated into La vacancies. The perovskite A (La) site is specially appropriate to detect lattice distortions in the surrounding MnO_6 octahedra, because slight changes in the charge geometry will significantly alter the electric field gradient (EFG) parameters.

The ^{111m}Cd probes decay to ^{111m}Cd through an intermediate state by the emission of two consecutive γ rays. The half-life for the ^{111m}Cd isomeric state is $T_{1/2}=48$ min, while

for the intermediate state is $T_{1/2}=84$ ns. The angular correlation between the two γ rays can be perturbed by both the EFG and the magnetic hyperfine field (MHF). These fields respectively couple to the nuclear electric quadrupole (Q) and the magnetic dipole ($\vec{\mu}$) moments of the intermediate nuclear state. The Hamiltonian for such static interactions, in the proper reference frame of the EFG tensor V_{ij} with $|V_{zz}| \geq |V_{yy}| \geq |V_{xx}|$, reads

$$\mathcal{H} = \frac{\hbar \omega_0}{6} \left[3I_z^2 - I(I+1) + \frac{1}{2} \eta (I_+^2 + I_-^2) \right] + \vec{\mu} \cdot \vec{B}_{hf}, \quad (1)$$

where $\omega_0 = 3eQV_{zz}/[2I(2I-1)\hbar]$ is the fundamental precession frequency, I represents the nuclear spin of the probe intermediate state ($I=5/2$ for ^{111}Cd), $\eta = (V_{xx} - V_{yy})/V_{zz}$ is the EFG asymmetry parameter, and \vec{B}_{hf} is the magnetic hyperfine field.¹⁶ The perturbation of the γ - γ directional correlation is described by the experimental $R(t)$ function, where t is the time spent by the nucleus in the ^{111}Cd intermediate state. For a hyperfine interaction, $R(t)$ may be expanded as $R(t) = \sum A_{kk} G_{kk}(t)$ with A_{kk} being the angular correlation coefficients. The perturbation factor $G_{kk}(t)$ is the signature of the fields interacting with the probes: MHF and an EFG in the ferromagnetic phase and EFG alone for $T > T_c$. Below T_c , in the presence of the two fields, we apply combined interaction theory to obtain the MHF and EFG parameters. Above T_c , on the other hand, $G_{kk}(t)$ may be expressed as¹⁶

$$G_{kk}(t) = S_{k_0} + \sum_n S_{k_n} \cos(\omega_n t) e^{-\omega_n \delta t} \quad (2)$$

considering only pure electric quadrupole interactions. The frequencies ω_n and amplitudes S_{k_n} are determined by the \mathcal{H} diagonalization. For spin $I=5/2$, three frequencies are observable that are functions of ω_0 and η .¹⁷ The exponential term in Eq. (2) accounts for an attenuation of the $R(t)$ function that appears in all spectra. This effect is due to randomly distributed intrinsic vacancies and defects that produce a Lorentzian distribution of static EFGs with central value ω_0 and relative width δ . Independently, in manganites, short-range charge diffusion coupled to lattice distortions (polarons) can lead to EFG fluctuations. These fluctuations contribute to further attenuate $R(t)$ when their time scale is comparable to the lifetime of the PAC probe intermediate state. When the characteristic fluctuation time (τ) is shorter than the nuclear spin precession time ($2\pi/\omega_0$), the $R(t)$ function can be satisfactorily approximated by a single exponential damping term $e^{-\lambda t}$ multiplying the static expression (2) with $\lambda \propto \omega_0^2 \tau$.¹⁸

Some experimental $R(t)$ curves are displayed in Fig. 1 for the compound with $\Delta=0.12$. We find in the temperature range from 10 to 776 K the coexistence of three main local environments (u, d, r), i.e., three fractions of probes (f_u, f_d, f_r) interacting with different local EFG distributions. The environment r is detected by a low residual fraction of the Cd probes (5%), which is temperature independent. Its EFG parameters are approximately $V_{zz}^r \approx 102 \text{ V/\AA}^2$ and $\eta_r \approx 0.9$ at room temperature. This highly axial asymmetric EFG might be related to probes located at the vicinity of

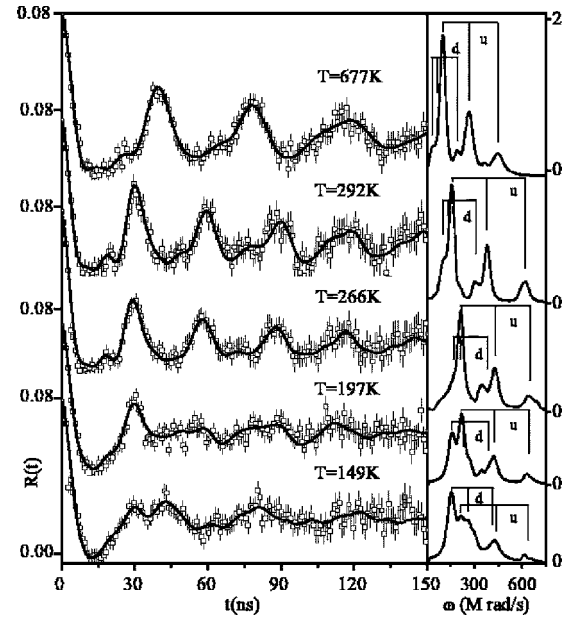


FIG. 1. Representative $R(t)$ experimental functions and the correspondent fits for $\text{LaMnO}_{3.12}$. Corresponding Fourier transforms are displayed on the right side.

Mn/La vacancies and/or other defects. Actually, assuming that the positions of the vacancies are not correlated, the probability that a Cd siting in a La vacancy has in its surroundings a Mn or next shell La vacancy is roughly 2%.

In Fig. 2, the temperature dependence of the EFG asymmetry parameter η (top) and principal component V_{zz} (bottom) for the u and d environments is displayed. For comparison, the EFG parameters found in $\Delta=0.08$ and $\Delta=0$ samples are also included in the same figure. The u environment that is dominant at high T shows an almost axially symmetric

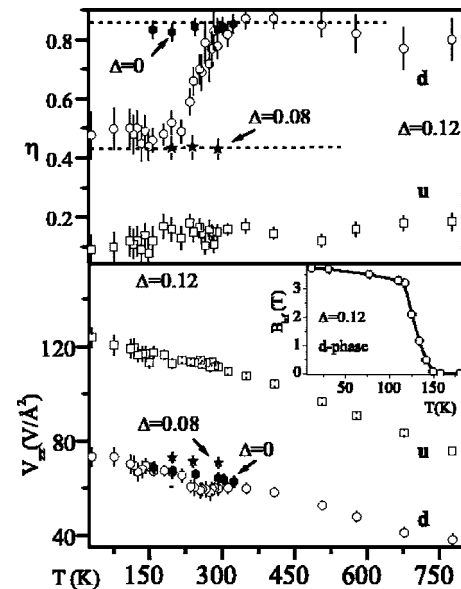


FIG. 2. Asymmetry parameter η (top) and EFG principal component V_{zz} (bottom) for $\text{LaMnO}_{3.12}$ as a function of T . EFG parameters for $\Delta=0.08$ and $\Delta=0$ are also shown. Inset: T dependence of the MHF for the d environment.

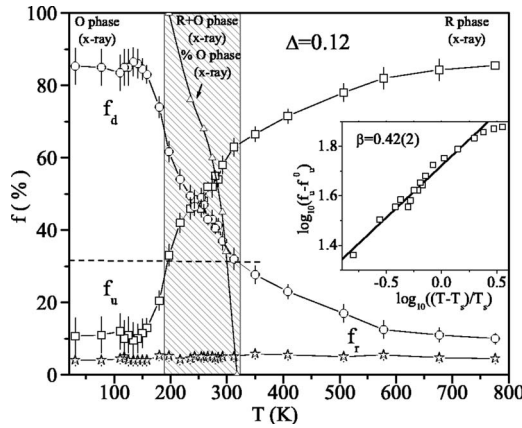


FIG. 3. Temperature dependence of the probe volume fractions f_u , f_d , and f_r . Triangles: orthorhombic phase percentage from x-ray diffraction. The shadowed region is limited by the temperatures where the percolation thresholds occur and the dashed horizontal line stands for the percolation threshold. Inset: log-log plot of $(f_u - f_u^0)$ vs $(T - T_s)$.

EFG ($\eta_u \approx 0$). This value characterizes an EFG with an axis of threefold or higher rotational symmetry, which is compatible with the rhombohedral lattice structure observed at high temperatures. The MnO_6 octahedra in the R structure are constrained by symmetry to be JT undistorted (equal Mn-O bond lengths), thus we will name this local environment *undistorted*. In contrast, the d (*distorted*) environment is characterized by a weaker V_{zz} (Ref. 19) and highly axial asymmetric EFG ($\eta_d > 0.45$). At high T , the values of η_d and V_{zz}^d coincide with the ones observed for the undoped fully JT-distorted orthorhombic system, $\Delta=0$, (full circles in Fig. 2). Consequently, at high temperatures, the d local environment must be characterized by a distortion involving several (minimum eight) Mn^{3+}O_6 octahedra similar to the collective JT-distorted lattice of the orbital-ordered LaMnO_3 .²⁰ Lowering T below 312 K, the asymmetry parameter η_d decreases stabilizing at a value close to that observed for the $\Delta=0.08$ sample (solid stars in Fig. 2). This behavior suggests that the JT distortions are weakening till they reach a similar degree as in the $\Delta=0.08$ sample. The EFG principal components V_{zz}^u and V_{zz}^d slightly increase with decreasing temperature. This is a typical feature of perovskite and related systems.²¹ Below $T_c \approx 145$ K both d and u local environments experience increasing magnetic hyperfine fields upon decreasing temperature (inset of Fig. 2), presenting at 10 K values of $B_{hf}^d = 3.8(2)T$ and $B_{hf}^u = 4.0(3)T$ compatible with a full ferromagnetic environment of the surrounding Mn ions.^{22,23}

Further insight into the behavior of d and u environments may be achieved by studying the T dependence of the volume fractions f_u and f_d . As may be seen in Fig. 3, the u environment is dominant at very high temperatures ($f_u \approx 86\%$ at $T=776$ K), though d regions survive up to that T ($f_d \approx 9\%$). This confirms the high stability of the inhomogeneous phase-segregated state. Our data, at high T , are compatible with a scenario where random distributed JT-distorted nanoclusters are embedded in an undistorted matrix as predicted by Refs. 10 and 24, setting a lower bound for the temperature where the polaron clusters start to form

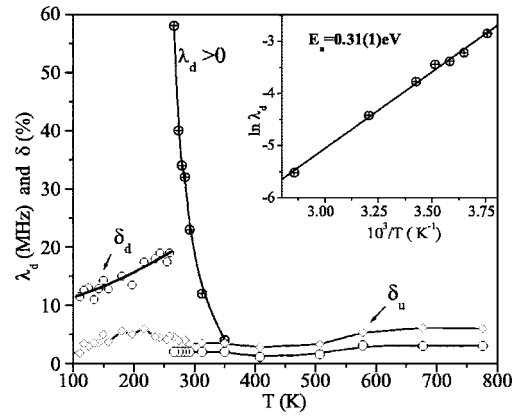


FIG. 4. Temperature dependence of static δ_d (○) and dynamic λ_d (⊕) attenuation parameters to the $R(t)$ function for the d environment. Static attenuation δ_u (◇) for the u environment. Inset: Arrhenius plot of λ_d to estimate the activation energy.

($T_{\text{clusters}} > 776$ K). At very low T , the fraction of the u environment reaches a remanent value ($f_u^0 \approx 10\%$), which is typically observed in CMR manganites²⁵ and is a signature of the ferromagnetic-metallic (FMM) and FMI phase coexistence. When the temperature changes, f_u (symmetrically f_d) suffers a smooth variation leading from an undistorted to a JT-distorted dominant microscopic environment. If we assume that this variation is a continuous phase transition, the order parameter would be $f_u - f_u^0$ and must follow a power law behavior $f_u - f_u^0 \sim (T - T_s)^\beta$ when the critical temperature T_s is approached from above. To check this possibility, we display f_u in a log-log plot in Fig. 3 (inset). The data adjust pretty well to a power law with $T_s \approx 170 \pm 10$ K (relatively close to T_c) and $\beta \approx 0.42 \pm 0.02$. Associated with the transition, there must also exist a correlation length, that must diverge at T_s . As may be seen in Fig. 2, when T decreases η_d starts to fall as the d component percolates [at $f_d \approx 31.16\%$ (Ref. 26)] and only stabilizes around T_s . Macroscopically, on the other hand, x-ray measurements detect a structural transition (R - O) that lies exactly between the temperatures corresponding to the percolation thresholds of the two main nanoscopic components. These are precisely the temperatures in which the minority invading cluster suffers a sudden size divergence becoming macroscopically observable.

The temperature dependence of the attenuation of $R(t)$ provides additional information about the dynamics of the u and d environments. A complete sketch of the dynamic and static attenuation for $R(t)$ in both environments is depicted in Fig. 4. The best fit to the $R(t)$ spectra discards the presence of time-dependent interactions for the u environment ($\delta_u \approx 4\%$ independently of T and $\lambda_u = 0$). Thus, in all temperature ranges, the charge transfer between Mn^{3+} and Mn^{4+} (activated hopping) in this environment should occur with a frequency higher than we can probe. For the d environment, on the other side, the best fits were obtained admitting a fluctuating EFG ($\lambda_d \neq 0$ and $\delta_d = 2\%$) in the temperature region spanning from $T=266$ to $T=350$ K. Notice that these time-dependent effects cannot be attributed to Cd/O and/or defects diffusion because they would be detected in both

fractions. The temperature dependence of the dynamic attenuation parameter, λ_d , allows us to estimate an activation energy E_a . This energy is obtained from $\lambda_d = \lambda_\infty e^{E_a/kT}$, and was found to be $E_a \approx 0.31$ eV (see the inset of Fig. 4), close to the polaron binding energy reported in the literature for low-doped manganites.^{27,28} We identify such EFG fluctuations with polaron diffusion related to charge (hole) transport. The EFG fluctuation time (τ) can be estimated from the maximum of $\lambda_d(T)$.²⁹ Considering that a carrier (hole) can hop to any of the eight octahedra around a La site (eight possible EFG states), we find $\tau = 0.5 \mu\text{s}$ at $T = 266$ K corresponding to ultraslow polaron diffusion. Similar polaron residence times have been recently reported in Ref. 22, although the E_a measured there was smaller possibly due to the intense magnetic field (7 T) needed to perform the NMR measurements. The competition of the distinct dynamics of the u (fast hopping) and d (related to polaronic conduction) environments is responsible for the macroscopic ferromagnetic insulator behavior observed in these systems.²⁵ Below T_c , both local environments become ferromagnetic and a phase coexistence between metallic (u) and insulator (d) regions exists. However, the majority fraction (d) is characterized by the ultraslow diffusion of charge carriers imposing an overall insulator behavior.

In conclusion, we report an extensive nanoscopic analysis on the prototypical FMI manganite $\text{LaMnO}_{3.12}$ using γ - γ

PAC spectroscopy. The undeniable separation of two distinct local environments, consistent with a phase coexistence scenario, allowed us to study the detailed structure, stability, and evolution of the JT-polaron clusters in manganites. We find that uncorrelated JT-polaron clusters survive up to a remarkably high T within the R crystallographic phase. Our results define a lower bound for the polaron cluster formation temperature ($T_{\text{clusters}} \geq 776$ K). When T is lowered, PAC measurements reveal a smooth increase in the JT-distorted nanoscopic environment density until it becomes dominant. This change may be described as a continuous phase transition with the transition temperature T_s , marking the point where the polaron cluster correlation length diverges. In parallel, a macroscopically O - R structural transition takes place as a consequence of the microscopic changes; actually it occurs between the percolation thresholds of the two main local components.

The authors thank W. Troeger, E. Rita, U. Wahl, J. M. López, R. Valiente, J. Vieira, and R. Catherall for fruitful discussions. This work was funded by the Portuguese Research Foundation (FCT), FEDER (Contract No. POCTI/FP/FNU/50183/2003, Contract No. POCTI/FP/FNU/50145/2003, and the EU Large Scale Facility Contract No. HPRI-CT-1999-00018. J.J.R. received partial funding from the NSF under Grant No. 0312510. A.M.L.L. thanks the FCT for her grant.

*Electronic address: armandina.lima.lobes@cern.ch

¹C. Zener, *Phys. Rev.* **82**, 403 (1951).

²A. J. Millis, P. B. Littlewood, and B. I. Shraiman, *Phys. Rev. Lett.* **74**, 5144 (1995).

³S. J. L. Billinge, R. G. DiFrancesco, G. H. Kwei, J. J. Neumeier, and J. D. Thompson, *Phys. Rev. Lett.* **77**, 715 (1996).

⁴G. M. Zhao, K. Conder, H. Keller, and K. A. Muller, *Nature (London)* **381**, 676 (1996).

⁵D. Louca, T. Egami, E. L. Brosha, H. Röder, and A. R. Bishop, *Phys. Rev. B* **56**, R8475 (1997).

⁶V. Kiryukhin, T. Y. Koo, H. Ishibashi, J. P. Hill, and S.-W. Cheong, *Phys. Rev. B* **67**, 064421 (2003).

⁷L. Martín-Carrón, A. de Andrés, M. J. Martínez-Lope, M. T. Casais, and J. A. Alonso, *Phys. Rev. B* **66**, 174303 (2002).

⁸N. Mannella, A. Rosenhahn, C. H. Booth, S. Marchesini, B. S. Mun, S.-H. Yang, K. Ibrahim, Y. Tomioka, and C. S. Fadley, *Phys. Rev. Lett.* **92**, 166401 (2004).

⁹V. Kiryukhin, A. Borissov, J. S. Ahn, Q. Huang, J. W. Lynn, and S.-W. Cheong, *Phys. Rev. B* **70**, 214424 (2004).

¹⁰E. Dagotto, *New J. Phys.* **7**, 67 (2005).

¹¹C. H. Booth, F. Bridges, J. J. Neumeier, E. L. Brosha, T. H. Geballe, G. J. Snyder, and G. H. Kwei, *J. Supercond.* **12**, 295 (1999).

¹²C. Ritter, M. R. Ibarra, J. M. De Teresa, P. A. Algarabel, C. Marquina, J. Blasco, J. García, S. Oseroff, and S.-W. Cheong, *Phys. Rev. B* **56**, 8902 (1997).

¹³F. Prado, R. D. Sanchez, A. Caneiro, M. T. Causa, and M. Tovar, *J. Solid State Chem.* **146**, 418 (1999).

¹⁴J. A. M. van Roosmalen and E. H. P. Cordfunke, *J. Solid State Chem.* **110**, 109 (1994).

¹⁵T. Butz, S. Saibene, T. Fraenzke, and M. Weber, *Nucl. Instrum.*

Methods Phys. Res. A **284**, 417 (1989).

¹⁶G. Schatz and A. Weidinger, *Nuclear Condensed Matter Physics* (Wiley & Sons, Ltd., Sussex, 1996).

¹⁷T. Butz, *Hyperfine Interact.* **52**, 189 (1989).

¹⁸A. Baudry and P. Boyer, *Hyperfine Interact.* **35**, 803 (1987).

¹⁹Note that the fact that $V_{zz}^d < V_{zz}^u$ alone does not imply that d has a higher symmetry.²¹

²⁰After Sternheimer corrections our EFG parameters agree with the results reported in the literature on the undoped compound using NMR (Ref. 22) and from *ab initio* FLAPW calculations [P. Ravindran (private communication)].

²¹R. Dogra, A. C. Junqueira, R. N. Saxena, A. W. Carbonari, J. Mestnik-Filho, and M. Moralles, *Phys. Rev. B* **63**, 224104 (2001).

²²G. Allodi, M. C. Guidi, R. De Renzi, A. Caneiro, and L. Pinsard, *Phys. Rev. Lett.* **87**, 127206 (2001).

²³M. K. Gubkin, T. A. Khimich, E. V. Kleparskaya, T. M. Perekalina, and A. V. Zalesky, *J. Magn. Magn. Mater.* **154**, 351 (1996).

²⁴E. Dagotto, T. Hotta, and A. Moreo, *Phys. Rep.* **344**, 1 (2001).

²⁵M. M. Savosta, V. I. Kamenev, V. A. Borodin, P. Novak, M. Maryska, J. Hejtmanek, K. Dorr, and M. Sahana, *Phys. Rev. B* **67**, 094403 (2003); M. M. Savosta and P. Novák, *Phys. Rev. Lett.* **87**, 137204 (2001).

²⁶D. Stauffer and A. Aharony, *Introduction to Percolation Theory* (Taylor & Francis, London, 1992).

²⁷A. Weisse, J. Loos, and H. Fehske, *Phys. Rev. B* **68**, 024402 (2003).

²⁸J. S. Zhou and J. B. Goodenough, *Phys. Rev. B* **68**, 144406 (2003).

²⁹H. Winkler and E. Gerdau, *Z. Phys.* **262**, 363 (1973).